Large-Scale Synthesis of Aligned Carbon Nanotubes Using $FeCl_3$ as Floating Catalyst Precursor

Haoqing Hou,[†,§] Andreas K. Schaper,[*,‡] Zeng Jun,[†] Frank Weller,[†] and Andreas Greiner[†]

Materials Science Center, Department of Chemistry and Department of Geosciences, Philipps University Marburg, Hans-Meerwein-Strasse, 35032 Marburg, Germany

Received September 24, 2002. Revised Manuscript Received November 27, 2002

The continuous interest in carbon nanotubes (CNTs) and nanotube arrays has led us to discover new routes of high-yield and low-cost synthesis of CNTs with controlled tube structure. Here we show that a dilute solution of $FeCl_3$ in toluene and *N*,*N*-dimethylamino-acetate is a high-efficiency floating catalyst precursor in a chemical vapor deposition process. The growth structure and the self-assembling behavior of the resulting multiwall tubes was characterized using scanning and transmission electron microscopy. Clear indications are provided of the participation of iron carbide in the tube formation at higher temperatures. The characteristic cone-shaped morphology of the tubes is described in detail and discussed in terms of its interesting practical implications.

1. Introduction

In the past decade, the synthesis of multiwall carbon nanotubes (MWCNTs) has attracted intense interest because of the potential applications of MWCNTs for electronic devices,[1] nanomechanical systems,[2] electrochemical energy storage and production,[3−5] scanning probes and sensors,[6−9] field emission sources,[10−15] and composite materials.[16−20] Various methods to grow CNTs have been developed (see the recent review article[21]) including arc-discharge,[22,23] laser ablation,[24] and chemical vapor deposition (CVD).[25−28] One of the remarkable advantages of the CVD method is that it allows achievement of high CNT yields, high purity, and excellent self-assembling of the nanotubes, if desired. Distinguished variants of this technique are plasma-enhanced CVD,[27] template CVD,[29] CVD on a preformed substrate,[12] and CVD using floating catalyst (CVD-ufc).[15,30−38] The CVD-ufc technique has been proven very effective in the synthesis of well-aligned and high-yield CNTs, in particular. Compared with other methods, this

* To whom correspondence should be addressed. Phone: +49 6421 282 3456. Fax: +49 6421 282 3383. E-mail: schaper@mailer.uni-marburg.de.
† Materials Science Center, Department of Chemistry.
‡ Materials Science Center, Department of Geosciences.
§ Present address: University of Akron, Ohio.

(1) Ho, G. W.; Wee, A. T. S.; Lin, J. *Appl. Phys. Lett.* **2001**, *79*, 260.
(2) Zheng, Q.; Jiang, Q. *Phys. Rev. Lett.* **2002**, *88*, 45503.
(3) Che, G.; Lakshmi, B. B.; Fisher, E. R.; Martin, C. R. *Nature* **1998**, *393*, 346.
(4) Cao, A.; Zhu, H.; Zhang, X.; Li, X.; Ruan, D.; Xu, C.; Wie, B.; Liang, J.; Wu, D. *Chem. Phys. Lett.* **2001**, *342*, 510.
(5) Frackowiak, E.; Béguin, F. *Carbon* **2002**, *40*, 1775.
(6) Dai, H.; Hafner, J. H.; Rinzler, A. G.; Colbert, D. T.; Smalley, R. E. *Nature* **1996**, *384*, 147.
(7) Dai, H.; Franklin, N.; Han, J. *Appl. Phys. Lett.* **1998**, *73*, 1508.
(8) Wong, S. S.; Jodelevich, E.; Woolley, A. T.; Cheung, C. L.; Lieber, C. M. *Nature* **1998**, *394*, 52.
(9) Stevens, R. M. D.; Frederick, N. A.; Smith, B. L.; Morse, D. E.; Stucky, G. D.; Hansma, P. K. *Nanotechnology* **2000**, *11*, 1.
(10) de Heer, W. A.; Châtelain, A.; Ugarte, D. *Science* **1995**, *270*, 1179.
(11) Rinzler, A. G.; Hafner, J. H.; Nikolaev, P.; Lou, L.; Kim, S. G.; Tomanek, D.; Nordlander P.; Colbert, D. C.; Smalley R. E. *Science* **1995**, *269*, 1550.
(12) Fan, S.; Chapline, M. G.; Franklin, N. M.; Tombler, T. W.; Cassell, A. M.; Dai, H. *Science* **1999**, *283*, 512.
(13) Sohn, J. I.; Lee, S.; Song, Y.-H.; Choi, S.-Y.; Cho, K.-I.; Nam, K.-S. *Curr. Appl. Phys.* **2001**, *1*, 61.
(14) Cao, A.; Ci, L.; Li, D.; Wei, B.; Xu, C.; Liang, J.; Wu., D. *Chem. Phys. Lett.* **2001** *335*, 150.
(15) Bonard, J.-M.; Croci, M.; Klinke, C.; Kurt, R.; Noury, O.; Weiss, N. *Carbon* **2002**, *40*, 1715.
(16) Calvert, P. *Nature* **1992**, *357*, 365.
(17) Treacy, M. M. J.; Ebbesen, T. W.; Gibson, J. M. *Nature* **1996**, *381*, 678.
(18) Dai, L.; Mau, A. W. H. *Adv. Mater.* **2001**, *13*, 899.
(19) Salvetat-Delmotte, J.-P.; Rubio, A. *Carbon* **2002**, *40*, 1729.
(20) Kashiwagi, T.; Grulke, E.; Hilding, J.; Harris, R.; Awad, W.; Douglas, J. *Macromol. Rapid Commun.* **2002**, *23*, 761.
(21) Huczko, A. *Appl. Phys. A* **2002**, *74*, 617.
(22) Iijma, S. *Nature* **1991**, *354*, 56.
(23) Journet, C.; Maser, W. K.; Bernier, P.; Loiseau, A.; de la Chapelle, M. L.; Lefrant, S.; Lee, R.; Fischer, J. E. *Nature* **1997**, *388*, 756.
(24) Rinzler, A. G.; Liu, J.; Dai, H.; Nikolaev, P.; Huffman, C. B.; Rodriguez-Macias, F. J.; Boul, P. J.; Lu, A. H.; Heyman, D.; Colbert, D. T.; Lee, R. S.; Fischer, J. E.; Rao, A. M.; Eklund, P. C.; Smalley, R. E. *Appl. Phys. A* **1998**, *67*, 29.
(25) Nikolaev, P.; Bronikowski, M. J.; Bradley, R. K.; Fohmund, F.; Colbert, D. T.; Smith, K. A.; Smalley, R. E. *Chem. Phys. Lett.* **1999**, *313*, 91.
(26) Ren, Z. F.; Huang, Z. P.; Xu, J. W.; Wang, D. Z.; Wen, J. G.; Xu, J. W.; Wang, J. H.; Calvet, L. E.; Chen, J.; Klemic, J. F.; Reed, M. A. *Appl. Phys. Lett.* **1999**, *75*, 1086.
(27) Ren, Z. F.; Huang, Z. P.; Xu, J. W.; Wang, H. J.; Bush, P.; Siegal, M. P.; Provencio, P. N. *Science* **1998**, *282*, 1105.
(28) Huang, Z. P.; Xu, J. W.; Ren, Z. F.; Wang, H. J.; Siegal, M. P.; Provencio, P. N. *Appl. Phys. Lett.* **1998**, *73*, 3845.
(29) Che, G.; Lakshmi, B. B.; Martin, C. R.; Fisher, E. R.; Ruoff, R. S. *Chem. Mater.* **1998**, *10*, 260.
(30) Andrews, R.; Jacques, D.; Rao, A. M.; Derbyshire, F.; Qian, D.; Fan, X.; Dickey, E. C.; Chen, J. *Chem. Phys. Lett.* **1999**, *303*, 467.
(31) Rao, C. N. R.; Sen, R.; Satishkumar, B. C.; Govindaraj, A. *Chem. Commun.* **1998**, *15*, 1525.
(32) Cheng, H. M.; Li, F.; Su, G.; Pan, H. Y.; He, L. L.; Sun, X.; Dresselhaus, M. S. *Appl. Phys. Lett.* **1998**, *72*, 3282.
(33) Rao, A. M.; Jacques, D.; Haddon, R. C.; Zhu, W.; Bower, C.; Jin, S. *Appl. Phys. Lett.* **2000**, *76*, 3813.
(34) Huang, S.; Dai, L.; Mau, A. W. H. *J. Phys. Chem. B* **1999**, *103*, 4223.
(35) Li, D. C.; Dai, L.; Huang, S.; Mau, A. W. H.; Wang, Z. L. *Chem. Phys. Lett.* **2000**, *316*, 349.
(36) Satishkumar, B. C.; Govindaraj, A.; Rao, C. N. R. *Chem. Phys. Lett.* **1998**, *307*, 158.

10.1021/cm020970g CCC: $25.00
Published on Web 01/04/2003

technique avoids drawbacks such as noncontinuous operation, special time-consuming preparation, or the activation of a catalyst-impregnated material.

Up to now, ferrocene,[30,39] $Fe(CO)_5$,[36−38] and iron-(II)-phthalocyanine (PcFe)[34,35] have been the compounds commonly used as floating catalyst precursors. In some cases, to make CNTs, additional carbon sources must be included because of the low carbon-to-iron ratio within the pure precursor compound. It is generally recognized that during high-temperature gas-phase pyrolysis the precursor is decomposed and reduced, by the hot H_2 atmosphere, to metallic iron in the form of nanosized particles and ultrafine particle aggregates. Whether, however, the subsequent filamentous carbon and carbon tube growth is monitored by metallic iron (α-Fe), or triggered by an intermediate iron carbide phase (FeC, Fe_2C, Fe_3C, Fe_7C_3) as the active catalyst,[40−42] is still a matter of debate.

Among the great variety of different morphologies of tubular carbon species, conical shapes[43−45] and bamboo-like structures[35,46−48] are frequently observed features. The formation of these types of morphologies is influenced by a large number of parameters. Cones can be made from a continuous graphene sheet by the introduction of pentagons and heptagons into the hexagonal graphitic network.[49−52] In the presence of a catalyst, the catalyst particles have to be considered as taking part in the formation of the pentagon/heptagon pairs.[49] Also, the transverse graphitic bridging of bamboo-structured tubes appears to be a direct consequence of the catalyst activity, so also is the formation of the rather exotic coiled CNTs.[53,54] Altogether, the details of the particular catalytic mechanisms of the various morphological formations are not yet fully understood.

Recently, transition metal salts such as iron(III) nitrate have been explored in the CVD synthesis and determined to be well-suited to catalyze the growth of oriented nanotubes.[55,56] In the present paper we report, for the first time, the application of iron(III) chloride as a floating catalyst precursor and show its effectiveness in the formation of multiwall CNTs and CNT arrays. Because $FeCl_3$ is a non-carbonaceous compound, we have introduced toluene to serve as the essential carbon source in the pyrolysis process. Large-scale, highly ordered MWCNT arrays were achieved, with tube morphologies ranging from straight to cone-shaped and regularly coiled. Detailed transmission electron microscope and electron diffraction observations could be related to particular growth mechanisms contributing to the filamentous tube formation. Special attention was paid to the nature of the catalyst activity as well as to the particulars of the conical growth characteristics.

Table 1. Operating Conditions and Product Parameters of the Synthesis of MWCNTs by Vapor Pyrolysis of a Toluene/DMAc Solution of $FeCl_3$

run	gas (flow 350−400 mL/min)	pyrolysis temp. (°C)	$FeCl_3$ conc. (wt. %)	fed solution (mL)	tube yield (mg)	tube diam. (nm)
A	Ar	650−750	0.5	30		
B	H_2	750−850	0.5	30	1278	100−250
C	H_2	650−750	0.5	30	896	30−150
D	H_2	600−700	0.5	30	645	10−100

2. Experimental Section

The experimental setup was identical to the equipment used for the catalytic gas-phase growth of MWCNTs based on ferrocene that was reported previously.[39] A 0.5 wt % solution of $FeCl_3$ in toluene and *N*,*N*-dimethylaminoacetate (DMAc), which is a good solvent accelerator, was fed into a two-stage tubular quartz reactor (inner diameter 35 mm, effective heating length 650 mm) at a rate of about 0.3 mL/min along with a H_2 flow of 350−400 mL/min. The quartz reactor was equipped with a dual furnace and independent temperature controllers. In the first stage, the solution was vaporized at 350−400 °C, far beyond its boiling temperature, then it was carried by the H_2 flow into the second reactor stage, where $FeCl_3$ became reduced to Fe in the hot H_2 stream at temperatures above 600 °C. Simultaneously, the vapor of toluene and DMAc was cracked, thereby liberating C_n and CH_n species. MWCNT growth was initiated at nanosized iron entities precipitated either on the silicon substrate or on the quartz surface of the reactor wall; from there the CNT arrays were scraped off as mat-like lumps. The starting material components, pyrolysis temperature, yield, and average tube diameter are listed in Table 1.

Characterization of the CNTs was performed by scanning electron microscopy (SEM) using a CamScan 4DV at 15 kV accelerating voltage, equipped with a NORAN energy-dispersive X-ray (EDX) detector, as well as by transmission electron microscopy (TEM) using a JEM 3010 operated at 300 kV. Raman spectroscopy measurements were carried out using a Jobin-Yvon LABRAM HR800 with 514.5-nm Ar laser excitation.

3. Results

The CVD-ufc synthesis of CNTs has usually been performed using a hydrogen/argon gas mixture in connection with one of the above-mentioned catalyst precursors. Pure Ar gas is not able to reduce the catalyst

(37) Hafner, J. H.; Bronikowski, M. J.; Azamian, B. R.; Nikolaev, P.; Rinzler, A. G.; Colbert, D. T.; Smith, K. A.; Smalley, R. E. *Chem. Phys. Lett.* **1998**, *296*, 195.
(38) Rohmund, F.; Falk, L. K. L.; Campbell, E. E. B. *Chem. Phys. Lett.* **2000**, *328*, 369.
(39) Hou, H.; Schaper, A. K.; Weller, F.; Greiner, A. *Chem. Mater.* **2002**, *14*, 3990.
(40) Oberlin, A.; Endo, M.; Koyama, T. *J. Cryst. Growth* **1976**, *32*, 335.
(41) Kock, A. J. H. M.; de Bokx, P. K.; Boellaard, E.; Klop, W.; Geus, J. W. *J. Catal.* **1985**, *96*, 468.
(42) Baker, R. T. K. *Carbon* **1989**, *27*, 315.
(43) Audier, M.; Oberlin, A.; Coulon, M. *J. Cryst. Growth* **1982**, *57*, 524.
(44) Boellaard, E.; de Bokx, P. K.; Kock, A. J. H. M.; Geus, J. W. *J. Catal.* **1985**, *96*, 481.
(45) Blank, V. D.; Polyakov, E. V.; Kulnitskiy, B. A.; Nuzhdin, A. A.; Alshevskiy, Y. L.; Bangert, U.; Harvey, A. J.; Davock, H. J. *Thin Solid Films* **1999**, *346*, 86.
(46) Lee, C. J.; Park, J. *Appl. Phys. Lett.* **2000**, *77*, 3397.
(47) Terrones, M.; Grobert, N.; Terrones, H. *Carbon* **2002**, *40*, 1665.
(48) Saito, Y. *Carbon* **1995**, *33*, 979.
(49) Murakami, H.; Hirakawa, M.; Tanaka, C.; Yamakawa, H. *Appl. Phys. Lett.* **2000**, *76*, 1776.
(50) Krishnan, A.; Dujardin, E.; Treacy, M. M. J.; Hugdahl, J.; Lynum, S.; Ebbesen, T. W. *Nature* **1997**, *388*, 451.
(51) Ajayan, P. M.; Ichihashi, T.; Iijima, S. *Chem. Phys. Lett.* **1993**, *202*, 384.
(52) Iijima, S.; Ichihashi, T.; Ando, Y. *Nature* **1992**, *356*, 776.
(53) Amelinckx, S.; Zhang, X. B.; Bernaerts, D.; Zang, X. F.; Ivanov, V.; Nagy, J. B. *Science* **1994**, *265*, 635.
(54) Bernaerts, D.; Zhang, X. B.; Zang, X. F.; Amelinckx, S.; van Tendeloo, G.; van Landuyt, J.; Ivanov, V.; Nagy, J. B. *Philos. Mag. A* **1995**, *71*, 605.
(55) Mauron, Ph.; Emmenegger, Ch.; Züttel, A.; Nützenadel, Ch.; Sudan, P.; Schlapbach, L. *Carbon* **2002**, *40*, 1339.
(56) Kind, H.; Bonard, J.-M.; Emmenegger, Ch.; Nilsson, L.-O.; Hadi, K.; Maillard-Schaller, E.; Schlapbach, L.; Forró, L.; Kern, K. *Adv. Mater.* **1999**, *11*, 1285.

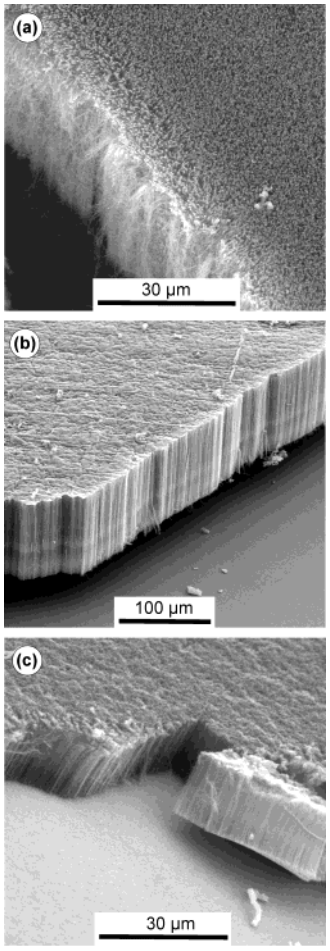

Figure 1. Scanning electron micrographs of MWCNT arrays produced by vapor pyrolysis of a toluene/DMAc solution of $FeCl_3$ within a temperature region of (a) 750−850 °C (sample B), (b) 650−750 °C (sample C), and (c) 600−700 °C (sample D).

so that in experimental run A (Table 1) no CNTs but only amorphous carbon particles have been formed. On the other hand, runs B, C, and D using pure H_2 flow are proved highly efficient in forming well-aligned CNTs. The SEM micrographs displayed in Figure 1 give clear evidence of the array character of self-assembled nanotube arrangements achieved at pyrolysis temperatures between 600 and 850 °C. Within a certain temperature range the arrays possess almost constant layer thickness, i.e., equal tube lengths. They extend over several square centimeters and are up to 100 μm thick. TEM observations show that with increasing pyrolysis temperature there is a tendency toward systematically increasing average tube diameter; the results of the TEM measurements are given in Table 1 for the different growth conditions, along with an estimation of the general yield of nanotubes.

Raman characterization of the pyrolyses products reveals the typical features of MWCNTs (Figure 2) without any significant differences among samples B to D. The spectrum exhibits the peak frequencies of the graphite (G) mode at 1576 cm^{-1} and contains disorder modes at 1351 cm^{-1} (D) and 1613 cm^{-1} (D') along with their overtones at 2693 cm^{-1} ($2 \times D$) and 3224 cm^{-1} ($2 \times D'$). The line at 2934 cm^{-1} is attributed to a combination of the graphitic and a disorder mode ($G + D$). [57]

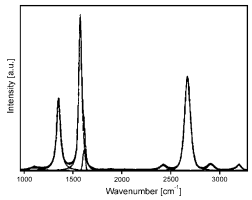

Figure 2. Raman spectrum of sample B (750−850 °C), which is also representative for similar characteristic spectra of the lower-temperature samples C and D.

Closer inspection, using scanning electron microscopy, of a nanotube array surface in the side view reveals a transversely oriented ripple pattern as shown in Figure 3a. By comparison with the TEM image in Figure 3b, bamboo-like structuring of the tubes can be made responsible for the appearance of the ripple pattern. A rather regular spacing of transverse carbon bridges inside a single tube and the lateral alignment of the bridges across several tubes give rise to this transversely extended structure. The catalyst particles were typically found located at the topside ends of the CNT arrays as shown in the TEM micrograph of sample C in Figure 3c. The inserted nanobeam electron diffraction pattern of a selected particle can be attributed to the ⟨111⟩ pole pattern of alpha-iron (ferrite). The precise orientation relationship between the particle and the corresponding tube direction, however, must remain unclear from this diffraction pattern.

Figure 4a illustrates that, besides the bamboo-type morphology, tubes occur even without indications of a transverse carbon bridge structure. As to the catalyst particle at the top of the hollow tube, lattice imaging reveals a set of lattice fringes parallel to the tube axis separated by approximately 1.9 Å (Figure 4b). The evaluation of the high-resolution structure image in Figure 6 suggests that they belong to an Fe_3C iron carbide phase. Generally, the catalyst particles at the tops of the CNTs show a drop-like shape up to a regular conical shape with the cone and tube axes almost coinciding, and with the larger diameter always facing outward (Figure 4a,c). The particles are entirely encapsulated by graphene sheets, the number of which is usually smaller at the top and bottom particle surfaces than in the side walls (Figure 4c−f). Obviously, the extent of the segmentation of the tubes by transverse carbon bridging is closely related to the cone character of the tubes. A general estimate is the following: the larger the semi-apex angle of the cone the higher the number of transverse sheets. Several fixed semi-apex angles were observed, namely 5, 10, and 20°, with corresponding sheet numbers increasing from 3 to about 20. In connection with this, it is important to notice the tapering of the inner cone segments in Figure 4c−g down to a diameter clearly smaller than the smallest diameter of the respective particle cone. From that observation it is evident that the nanotube walls must have grown inward in the radial direction while the catalyst particles have become lifted up during the growth.

The graphene layers in a perfect cone-shaped MWCNT are of finite width, they terminate at the inner and outer

(57) Li, W.; Zhang, H., Wang, Ch.; Zhang, Y.; Xu, L.; Zhu, K.; Xie, S. *Appl. Phys. Lett.* **1997**, *70*, 2684.

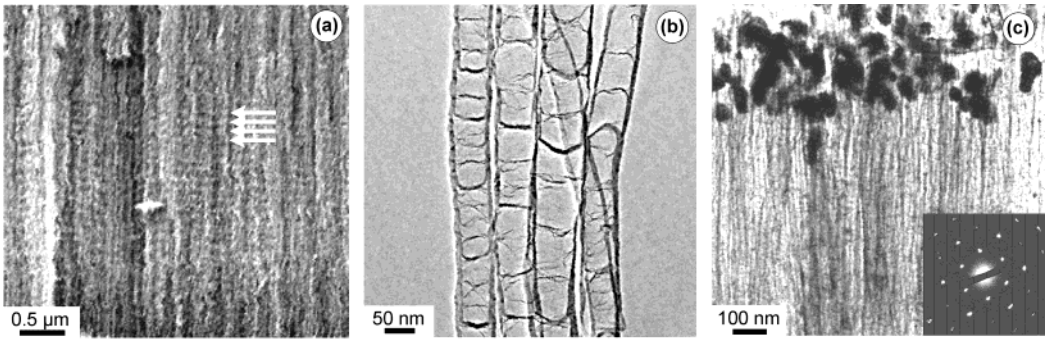

Figure 3. Electron micrographs of the overall nanotube structure of sample C: (a) SEM side-view of a nanotube array revealing a transverse patterning across the aligned MWCNTs (see arrows); (b) TEM close-up of a few nanotubes showing a bamboo-like morphology related to the pattern in (a); (c) array portion including the top layer with the catalyst particles, (111) nanobeam diffraction pattern of α-Fe inset.

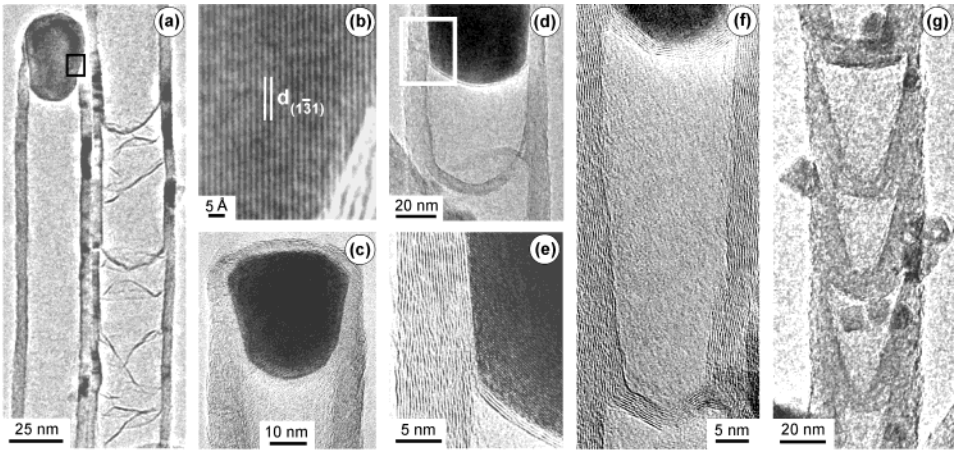

Figure 4. TEM micrographs of typical growth structures of sample B (750−850 °C) MWCNTs. (a) Tubes without and with transverse carbon bridging; (b) lattice plane image of the catalyst particle area marked in (a); (c) completely encapsulated cone-shaped particle; (d−g) compartments of bamboo-structured MWCNTs revealing different semi-apex angles of conical growth and related changes in the amount of transverse graphite bridging.

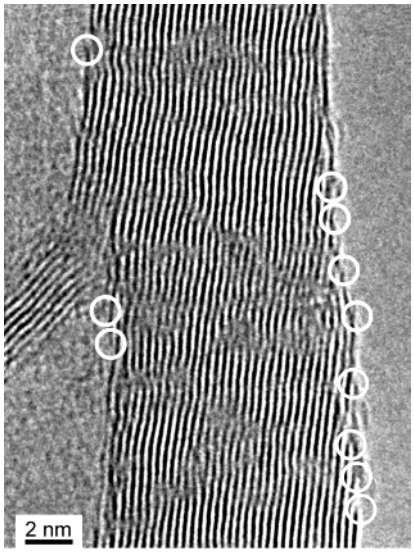

Figure 5. Lattice plane image showing a portion of a tube wall with a semi-apex angle of approximately 5°, and with the corresponding edges of terminating graphite sheets (open circles). On the left side the starting point of an inner graphite bridge can be seen.

tube surface. Numerous of those edges of terminating graphene sheets are resolved in Figure 5 which shows a close-up image of a tube wall, including part of a transverse bridge structure. In other surface areas the staggered edges are covered by irregular single carbon layers parallel to the tube axis.

Usually, the catalyst particles encapsulated in the nanotubes were completely single crystalline. Other than the bcc α-Fe identified in Figure 3c of sample C (650−750 °C), in the higher temperature sample B (750−850 °C) the occurrence of iron carbides has been observed. This carbide phase was proved by high-resolution structure imaging of a particle as shown in Figure 6 along with the power spectrum of the image. The micrograph provides the [310] zone axis view of the orthorhombic structure of cementite (Fe_3C); the axis of the encapsulating carbon tube coincides very precisely with the crystallographic $[1\bar{3}\bar{5}]$ axis of the Fe_3C. A lattice plane image of the carbide phase corresponding to the above orientation is given in Figure 4b.

Among the carbon nanomaterial obtained by the $FeCl_3$-mediated decomposition of toluene/DMAc, besides the dominating straight or conical tubes one finds also other morphological forms as, e.g., the coiled tube shown in Figure 7. On the average, the tube diameters in those helix-shaped forms vary between 10 and 50 nm, and the diameter of a helix, which almost equals the pitch hight, may range from about 50 to more than 200 nm. In Figure 7a the coiled tube runs parallel with a straight one and they touch each other periodically. The close-up in Figure 7b provides clear proof of the hollow tube

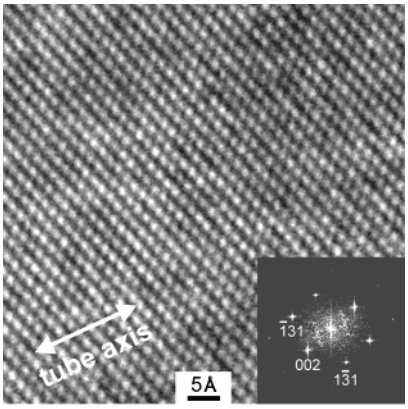

Figure 6. High-resolution TEM structure image of an Fe_3C catalyst particle seen along the [310] direction; inset is the power spectrum of the image (tube axis arrowed).

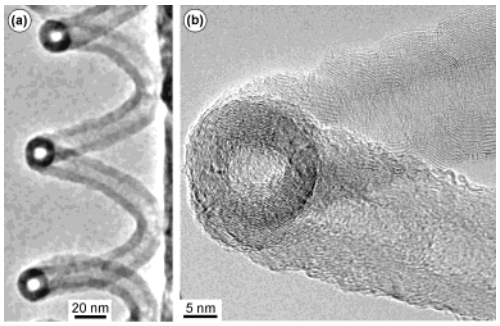

Figure 7. Portion of a helix-shaped MWCNT attached to the surface of a straight nanotube; (b) high magnification image of the cross-sectional ring pattern in the middle of (a).

character of the helix-shaped multiwall CNT which exhibits about 25 graphene layers.

4. Discussion

It is one important finding of this paper that large arrays of highly ordered multiwall carbon nanotubes can be grown by the pyrolysis of a solution of $FeCl_3$ in toluene/*N*,*N*-dimethylaminoacetate in a H_2 stream within a temperature range between 600 and 850 °C. The reaction temperature influences the CNT growth in a quantitative manner in two respects: it determines the diameter of the MWCNTs, and it controls their yield. It is suggested that large-diameter CNTs originate from large-sized catalytic particles, and vice versa.[35,37] It seems reasonable to assume that the reduction of $FeCl_3$ is especially effective at high temperature forming larger amounts of particles with large diameter, whereas a lower reaction temperature favors the formation of small diameter particles.

Two growth mechanisms are discussed in the literature:[40,53] tip growth and base growth, regarding the two possible pathways of carbon diffusion from above (through the upper small particle), and from below (through the supporting base particle). The results discussed here are concerned with the first of the two mechanisms. Accordingly, the deposition and extrusion of carbon occurs in the contact region between the small particle and the already formed tubule segment. In the course of this process the small catalyst particle is lifted away from the support due to the pressure exerted by the growth of the carbon layers along the axial tube direction as well as by the lateral inward growth of the tube wall. Thereby, the compressive forces cause the liquid (or quasi-liquid) metal particle to adopt a conical shape which will then further on determine the principal growth characteristics.

In a large number of cases, the CNTs synthesized in this work contain carbon bridges which span the lumen of the tubes giving them a bamboo-like appearance. If, temporarily, the local carbon flux is reduced, Figure 4a confirms how tube growth may go on without any further bridge formations. It can be observed that the carbon bridges are normally associated with conical growth characteristics of the CNTs. The fundamentals of nucleation and growth of graphitic cones has been discussed by Krishnan et al.,[50] Ajayan et al.,[51] and Iijima et al.[52] Cones can be made from a continuous graphene sheet by the introduction of pentagons into the hexagonal network leading to a limited number of fixed cone types. Conically shaped CNTs were first reported by Audier et al.;[43] their structure and formation mechanism have been analyzed recently by Blank et al.[45] Although nested cone structures with larger semi-apex angles (9.59, 19.47, 30, 42.3, and 56.5°) can be formed by the incorporation of pentagons,[50] a semi-apex angle of 4.78°[58] can be explained only by introducing heptagon/pentagon pairs.[45] The semi-apex angles of the nanotubes measured here are close to 5, 10, and 20° which very well agrees with the results of CNTs produced in a hot isotactic pressure apparatus.[45]

Heptagon/pentagon pairs, along with kink defects, are suggested to play the decisive role in the formation of more complex morphologies, such as the coiled MWCNTs found by Bernaerts et al.,[54] and in the present paper. On the other hand, it is known that van der Waals forces are able to induce radial elastic deformations of CNTs;[59] they may also explain the attractive interaction between a straight and a parallel nanotube as seen in Figure 7a and in examples given in the literature.[54]

It has been pointed out by Baker[42] and Boellard et al.,[44] and adopted later on in the growth models of Amelinckx et al.[53] and Saito,[48] that the key step in the catalytic growth of filamentous carbon is the diffusion of carbon species through the catalyst particle. Recent synthesis experiments of SWCNTs using Ni as catalyst by Gavillet et al.[60,61] suggest the ability of liquid Ni particles to incorporate a large amount of carbon, but a decrease of the carbon solubility limit upon cooling. Bulk diffusion of dissolved carbon through metal particles (Ni and Fe/Co) has, e.g., been described by Bengaard et al.[62] and Holstein.[63] We suppose that such a diffusion mechanism also contributes to the establishment of the transverse carbon bridges which cross the MWCNT walls at intervals lending the tubes a bamboo-like shape. The absorbed carbon is excreted at the bottom

(58) Amelinckx, S.; Devouard, B.; Baronnet, A. *Acta Crystallogr. A* **1996**, *52*, 850.
(59) Ruoff, R. S.; Tersoff, J.; Lorents, D. C.; Subramoney, S.; Chan, B. *Nature* **1993**, *364*, 514.
(60) Gavillet, J.; Loiseau, A.; Jounet, C.; Willaime, F.; Ducastelle, F.; Charlier, J.-C. *Phys. Rev. Lett.* **2001**, *87*, 275504.
(61) Gavillet, J.; Loiseau, A.; Ducastelle, F.; Thair, S.; Bernier, P.; Stéphan, O.; Thibault J., Charlier, J.-C. *Carbon* **2002**, *40*, 1649.
(62) Bengaard, H. S.; Nørskov, J. K.; Sehested, J.; Clausen, B. S.; Nielsen, L. P.; Molenbroek, A. M.; Rostrup-Nielsen, J. R. *J. Catal.* **2002**, *209*, 365.
(63) Holstein, W. L. *J. Catal.* **1995**, *152*, 42.

and the side of the particles and consecutively segregates as graphite without extended slippages of already formed layers.[42,48] In that view, thickness growth of the tubes occurs from the inside. A scenario that proposes the deposition of carbon from the inside at the contact region between the particle and the growing edge of the inner tubule is consistent with the growth of cone-shaped graphitic scrolls with definite chirality[64] as with a nested cone growth.[45] The tube growth proceeds discontinuously by accumulation of compressive stresses within the extending CNT compartment and jumping the particle to the top of the tube[48] when a certain threshold value is reached.

It is commonly thought that graphite layers completely covering the particle at the top of a tube inhibit further tip growth, and that any continuation of growth may presumably occur from the support.[35,40,44,53] On the other hand, one cannot exclude the possibility that metal atoms are able to penetrate through the capping graphite layers due to the high temperature treatment during pyrolysis. The frequently observed small particles adhering to the outer tip surface of a tube, sometimes facing an internally enclosed larger particle, may be interpreted as indications of a metal-through-carbon migration process. Clear proofs of such a migration have been given by the in situ studies of Banhart et al.,[65] and by Sinclair et al.,[66] and are confimed by our own experiments published elsewhere.[67]

Although the catalytic activity of metal particles in filamentous growth of carbon has been known previously,[40−44] the mechanisms of the catalytic process are not yet exactly clarified. Regarding the CVD-ufc technique for producing well-organized carbon nanotubes, until recently it has been an open question whether the metal or a metal carbide is the active entity. However, using microdiffraction and high-resolution imaging Sinclair et al.[65,68] proved the participation of the iron carbide phase cementite in the graphitization of amorphous carbon. The determining role of platelets of a metal carbide phase in the root growth mechanism of SWCNTs has been shown in HRTEM and energy filter transmission electron microscopy (EFTEM) studies of Gavillet et al,[69] and also in the metal−carbon interaction during iron-catalyzed CO decomposition described by Blanck et al.[70] as being accompanied by an α-Fe → Fe_3C transformation through an intermediate hexagonal ϵ-Fe/ϵ-Fe_xC phase. The evidence we have gained here of the presence of α-Fe in the medium-temperature MWCNTs, but Fe_3C particles in the high-temperature pyrolysis products, are in close agreement with these considerations. The migration and dissolution of carbon inside the metal particles is inherently linked with the carbide formation process.

5. Conclusions

In this paper a novel route of the synthesis of MWCNTs has been established using iron(III) chloride in a toluene/*N*,*N*-dimethylaminoacetate solution and 600−850 °C hot H_2 atmosphere as floating catalyst precursor. The decomposition products of toluene and DMAc serve as carbon sources for the CNT formation. Advantages of the new metal salt catalyst, such as easy availability and handling, nontoxicity, low price, and ease of volatilazation, even hold in combination with the toluene precursor which is less toxic than the widely used benzene. The iron atoms remaining after the reduction of $FeCl_3$ and precipitated on the substrate surface aggregate to nanoparticles which act as catalytic centers for the nanotube growth. Evidence was obtained that the catalytic mechanism involves a phase transition from metallic iron to iron carbide. The final synthesis products consist of up to 100-μm thick, large-scale, self-assembled arrays of well-aligned MWCNTs in the diameter range of 10−250 nm; the catalytic particles are located on the topside end of the CNTs. The nanotubes synthesized in this way show well-defined morphologies: either straight, slightly conical, or coiled. Excellent alignment of densely packed tubes within nanotube arrays is achieved as compared to similar array formations described in the literature.

The catalytic route described here may be of considerable practical importance in future CNT array production for application in electrical or magnetic devices. Furthermore, MWCNTs composed of cone-shaped graphitic sheets may turn out to be especially useful in the development of new intercalation compounds. The conical growth characteristics implies an "opening" of the graphitic layer structure of the nanotube walls: each single graphene layer, in case of a nested cone structure, or the edges of chiral graphene layers, in case of a scroll structure, terminate at the inner as well as the outer tube surface. As a consequence of this, the structure becomes more likely accessible to doping by electron donors or electron acceptors to control their electronic properties,[71,72] or to hydrogen storage by intercalation.[73]

CM020970G

(64) Ruland, W.; Schaper, A. K.; Hou, H.; Greiner, A. *Carbon*, in press.
(65) Banhart, F.; Redlich, Ph.; Ajayan, P. M. *Chem. Phys. Lett.* **1998**, *292*, 554.
(66) Sinclair, R.; Itoh, T.; Chin, R. *Microsc. Microanal.* **2002**, *8*, 288.
(67) Schaper, A. K.; Hou, H.; Greiner, A.; Schneider, R.; Phillipp, F. *Chem. Phys. Lett.*; submitted for publication.
(68) Itoh, T.; Sinclair, R. *Mater. Res. Soc. Symp. Proc.* **1995**, *382*, 45.
(69) Gavillet, J.; Loiseau, A.; Thibault, J.; Maigné, A.; Stéphan, O. *Proceedings ICEM-15, Durban, South Africa, September 1−6*, 2002; *Vol. 1*, p 201.
(70) Blank, V. D.; Kulnitskiy, B. A.; Batov, D. *Proc. EUREM 12, Brno, Czech Republic, July 9−14*, **2000**; p 239.
(71) Mordkovich, V. Z.; Baxendale, M.; Yoshimura, S.; Chang, R. P. H. *Carbon* **1996**, *34*, 1301.
(72) Duclaux, L. *Carbon* **2002**, *40*, 1751.
(73) Chambers, A.; Park, C.; Terry, R.; Baker, K.; Rodriguez, N. M. *J. Phys. Chem.* **1998**, *102*, 4253.